

Hybrid acceleration-impedance sensor nodes on Imote2-platform for damage monitoring in steel girder connections

Jeong-Tae Kim*, Jae-Hyung Park, Dong-Soo Hong and Duc-Duy Ho

Department of Ocean Eng., Pukyong National University, Busan, Korea

(Received October 18, 2010, Accepted April 13, 2011)

Abstract. Hybrid acceleration-impedance sensor nodes on Imote2-platform are designed for damage monitoring in steel girder connections. Thus, the feasibility of the sensor nodes is examined about its performance for vibration-based global monitoring and impedance-based local monitoring in the structural systems. To achieve the objective, the following approaches are implemented. First, a damage monitoring scheme is described in parallel with global vibration-based methods and local impedance-based methods. Second, multi-scale sensor nodes that enable combined acceleration-impedance monitoring are described on the design of hardware components and embedded software to operate. Third, the performances of the multi-scale sensor nodes are experimentally evaluated from damage monitoring in a lab-scaled steel girder with bolted connection joints.

Keywords: acceleration; impedance; hybrid; structural health monitoring; Imote2 sensor platform; multi-scale sensor node.

1. Introduction

Most large steel structures have structural connections such as bolted joints of beam structures. Potential damage types of the structural connections include fatigue cracks between bolt holes, the change in tensile force of bolts, and failures of connection components. Especially, Kyung *et al.* (2002) presented the damage statistics of connections for 100 steel girder bridges of Korea as: rivet falloff (49.3%), bolt loosening (42.6%), bolt fall-off (6.2%), bolt corrosion (1.7%), and failure of welded connection (0.1%). From the statistics, the major damage types of the connections in steel girder bridges occur at bolt and rivet connections rather than welded connections. Structural health monitoring (SHM) on those structural connections becomes an important topic since damage occurred in structural connections, which is not detected or remedied appropriately, may result in local failure, reduction of load carrying capacity, or catastrophic disaster.

Up to date, many studies have been focused on SHM of structural connections by using global and local dynamic characteristics (Lam *et al.* 1998, Yun *et al.* 2001, Sohn *et al.* 2003, Fasel *et al.* 2005, Kim *et al.* 2006b, Roh *et al.* 2005, Nagayama 2007, Mascarenas *et al.* 2009). To implement SHM systems for structural connections, however, the costs associated with installation and maintenance of SHM systems can be very high. The high costs associated with wired SHM systems can be

*Corresponding Author, Professor, E-mail: idis@pknu.ac.kr

greatly reduced through the adoption of wireless sensors. An advantage of wireless sensor is that the automated operation can be implemented by embedded operation software. This fact leads a new paradigm that adopts smart sensors for autonomous and cost-efficient SHM (Straser and Kiremidjian 1998, Spencer *et al.* 2004, Kurata *et al.* 2005, Lynch *et al.* 2004, Nagayama *et al.* 2007, Krishnamurthy *et al.* 2008, Cho *et al.* 2008, Taylor *et al.* 2009, Rice *et al.* 2010).

Straser and Kiremidjian (1998) first proposed a design of a low-cost wireless modular monitoring system (WiMMS) for SHM applications. Since then, many researchers have developed their own wireless sensor nodes or used commercialized sensor platforms. Lynch *et al.* (2006) improved the performance of WiMMS in which acceleration-based damage monitoring algorithms are embedded. In addition, Zimmerman *et al.* (2008) and Weng *et al.* (2008) improved wireless functionalities of the WiMMS for output-only modal identification. Kurata *et al.* (2005) compared the performances of two Berkeley Motes, MICA and MICA2, for acceleration-based SHM of two-story building model. Nagayama *et al.* (2009) used Imote2 sensor platforms from Memsic Co. (2010) for acceleration-based SHM of truss structures. Meanwhile, Mascarenas *et al.* (2007) developed a wireless sensor node for impedance-based SHM. For multi-functional purpose, Sazonov *et al.* (2006) developed wireless sensor nodes named WISAN (wireless intelligent sensor and actuator network) for acceleration and dynamic strain measurements. Also, Park *et al.* (2010) developed acceleration-based and impedance-based smart sensor nodes (Acc-SSN and Imp-SSN) which are modified from the sensor nodes by Lynch *et al.* (2006) and Mascarenas *et al.* (2007), respectively.

The previous studies have been mainly focused on developing SHM systems by using a single physical quantity such as strain, acceleration or electro-mechanical impedance. However, the reliability of SHM systems using a single sensing device is relatively low compared to the case of multi-physical quantities. For example, a SHM method using global vibration is utilized to monitor the change in structural integrity by using a few sensors but cannot detect incipient small damage. Also, SHM methods using local impedance signatures are sensitive to small changes in local critical members but require many sensors to cover whole structure. Therefore, a hybrid SHM using multi-scale sensing mechanism can be an alternative approach (Studer and Peters 2004, Sim and Spencer 2007, Park *et al.* 2010).

In this study, hybrid acceleration-impedance sensor nodes on Imote2-platform are designed for damage monitoring in steel girder connections. Thus, the feasibility of the sensor nodes is examined about its performance for vibration-based global monitoring and impedance-based local monitoring in the structural systems. To achieve the objective, the following approaches are implemented. First, a damage monitoring scheme is described in parallel with global vibration-based methods and local impedance-based methods. Second, multiscale sensor nodes that enable combined acceleration-impedance features are described on the design of hardware components and embedded software to operate. Third, the performances of the multi-scale sensor nodes are experimentally evaluated from damage monitoring in a lab-scaled steel girder with bolted connection joints.

2. Damage monitoring scheme for steel girder connection

2.1 Design of damage monitoring scheme

Several researchers have proposed damage monitoring methods based on multi-scale sensing of changes in multi-physical quantities of structures. Studer and Peters (2004) proposed a methodology using strain, integrated strain, and strain gradients to monitor structural volumes. Kim *et al.* (2006a)

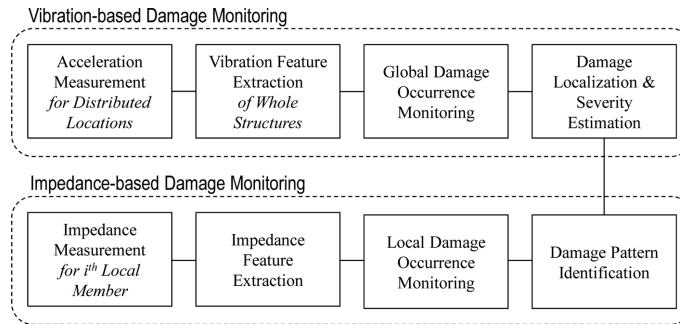


Fig. 1 Hybrid acceleration-impedance monitoring scheme

proposed a hybrid algorithm utilizing acceleration and impedance signatures to monitor cracks and failures of supports in plate-girder bridges. Sim and Spencer (2007) proposed a multi-scale approach to accommodate both acceleration and strain measurements simultaneously for SHM of truss structures. As a hybrid methodology, Kim *et al.* (2009) and Park *et al.* (2010) examined the applicability of the combined use of acceleration and impedance signatures for damage monitoring of structures.

On the basis of the hybrid acceleration-impedance monitoring concept, a damage monitoring scheme that can be implemented for steel girder connections is schematized in Fig. 1. Using the hybrid scheme, the vibration-based monitoring of damage is performed in global structure level and in parallel manner the impedance-based monitoring of damage is performed in local critical members. Firstly, vibration-based damage monitoring is performed in four steps: acceleration measurement for distributed locations, vibration feature extraction for entire structure, global damage occurrence monitoring, and damage localization and severity estimation. Secondly, impedance-based damage monitoring is also performed in four steps: impedance measurement for prescribed local members, impedance feature extraction, local damage-occurrence monitoring, and damage pattern identification.

2.2 Global vibration-based monitoring methods

Damage causes the change in structural parameters (i.e., mass, damping, and stiffness), which, in turn, results in the change in vibration responses of a structure. Two vibration-based damage monitoring methods were selected as follows: first, correlation coefficient (CC) of power spectral densities (PSDs) was selected to globally alert the occurrence of damage in the structural system; and next, modal strain-energy (MSE)-based damage index method was selected to detect the location of damage.

2.2.1 Correlation coefficient of power spectral densities (CC of PSDs)

Assume that two acceleration signals $x(t)$ and $y(t)$ are measured before and after a damaging episode, respectively. Their corresponding power spectral densities S_{xx} and S_{yy} are calculated from Welch's procedure as (Bendat and Piersol 2003)

$$S_{xx}(f) = \frac{1}{n_d T} \sum_{i=1}^{n_d} |X(f, T)|^2 \quad (1)$$

$$S_{yy}(f) = \frac{1}{n_d T} \sum_{i=1}^{n_d} |Y(f, T)|^2 \quad (2)$$

where X and Y are dynamic responses transformed into frequency domain; n_d is the number of divided segments; and T is data length of a divided segment.

The correlation coefficient of PSDs (CC of PSDs) represents the linear identity between the two PSDs obtained before and after a damage event.

$$\rho_{XY} = \frac{E|S_{xx}(f)S_{yy}(f)| - E|S_{xx}(f)|E|S_{yy}(f)|}{\sigma_{S_{xx}}\sigma_{S_{yy}}} \quad (3)$$

where $E[\cdot]$ is the expectation operator, and $\sigma_{S_{xx}}$ and $\sigma_{S_{yy}}$ are the standard deviations of PSDs of acceleration signals measured before and after damaging episode, respectively. If any damage occurs in the target structure, its acceleration responses would be affected and, consequently, the indication by the CC of PSDs can be a warning sign of the presence of damage. A control chart analysis is used to discriminate damage events from the CC values (Sohn *et al.* 2001). The lower control limit (LCL) is determined as

$$LCL_\rho = \mu_\rho - 3\sigma_\rho \quad (4)$$

where μ_ρ and σ_ρ are the mean and the standard deviation of the CC values, respectively. The occurrence of damage is indicated when the CC values are beyond (i.e., less than) the bound of the LCL; otherwise, there is no indication of damage occurrence. To use the CC of PSDs as a damage-sensitive index, it would be better to get rid of measurement uncertainty induced by inconsistent excitation conditions.

2.2.2 MSE-based damage localization index

Based on the earlier formulation proposed by Kim and Stubbs (1995), Kim *et al.* (2003) proposed an improved damage index method using changes in modal strain energies. For a flexural girder, damage in the j^{th} member is defined as the relative change between undamaged flexural stiffness, k_j , and damaged one, k_j^* , of the same element. Modal strain energy (MSE) is a damage sensitive feature using mode shape curvature. For all available vibration modes, the MSE-based damage index for the j^{th} location, β_j , is given by (Kim *et al.* 2003)

$$\beta_j = \frac{k_j}{k_j^*} = \frac{\sum_{i=1}^M \gamma_{ji}^*}{\sum_{i=1}^M (\gamma_i g_i + \gamma_{ji})} \quad (5)$$

where γ_i and γ_{ji} represent the i^{th} modal stiffness and the contribution of the j^{th} element to the i^{th} modal stiffness, respectively. Note the asterisk denotes the damaged state. To represent flexural modal strain energies and to estimate girder damage accordingly, γ_i , γ_i and γ_{ji}^* are formulated as follows (Kim *et al.* 2003): $\gamma_{ji} = \int_j [\phi_i''(x)]^2 dx$, $\gamma_{ji}^* = \int_j [\phi_i^{*''}(x)]^2 dx$, and $\gamma_i = \int_0^L [\phi_i''(x)]^2 dx$. The term $\phi_i''(x)$ is mode shape curvature of i^{th} modal vector and it is computed from i^{th} mode shape vector $\phi_i(x)$ which is measured vertically from the girder. The term g_i is a dimensionless factor representing the fractional changes in the i^{th} modal parameters (i.e., $g_i = \delta\omega_i^2/\omega_i^2$).

For damage localization practice, the damage indices are normalized according to the standard rule as

$$Z_j = (\beta_j - \mu_\beta) / \sigma_\beta \quad (6)$$

where μ_β and σ_β represent, respectively, the mean and standard deviation of the collection of β_j values. Then, the damage is localized from the statistical hypothesis tests. The null hypothesis (i.e., H_0) is taken to be the structure undamaged at j^{th} element and the alternate hypothesis (i.e., H_1) is taken to be the structure damaged at j^{th} element. In assigning damage to a particular location, the following decision

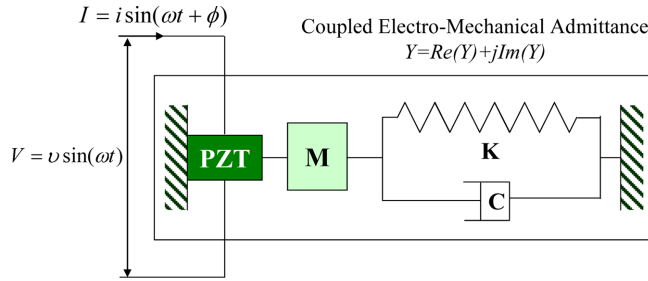


Fig. 2 1D Model of electro-mechanical interaction of piezoelectric patch and host structure (Liang *et al.* 1996)

rule is utilized: 1) choose H_1 if $Z_j \geq z_o$; and 2) choose H_0 if $Z_j < z_o$, where z_o is number which depends upon the confidence level of the localization test. Then damage is assigned to a particular location j if Z_j exceeds the confidence level.

2.3 Local impedance-based monitoring methods

Impedance-based SHM techniques utilize piezoelectric sensors (e.g., PZT or MFC patches) which are locally sensitive to its sensor-vicinity area. As shown in Fig. 2, the piezoelectric material is described by its short circuited mechanical impedance, which is powered by voltage or current (Liang *et al.* 1996). The host structure is modeled as the effect of mass, stiffness, damping, and boundary conditions. The electrical impedance of the piezoelectric patch bonded onto a host structure is directly related to the mechanical impedance of the structure. When damage occurs to a structure, its mechanical impedance would be changed. Hence, any changes (such as magnitude of admittance and resonant frequency) in the electrical impedance signature are attributed to damage or changes in mechanical property of the local sensor-vicinity zone (Giurgiutiu and Zagrai 2002, Bhalla and Soh 2004, Park *et al.* 2005, Park *et al.* 2006).

2.3.1 Root mean square deviation (RMSD) of impedance signatures

To quantify the change in impedance signature due to damage in the structure, the root-mean-square-deviation (RMSD) of impedance signatures measured before and after damage (Sun *et al.* 1995) is used in this study. The RMSD is calculated from impedance measurements before and after damage as

$$RMSD(Z, Z^*) = \sqrt{\frac{\sum_{i=1}^N [Z^*(\omega_i) - Z(\omega_i)]^2}{\sum_{i=1}^N [Z(\omega_i)]^2}} \quad (7)$$

where $Z(\omega_i)$ and $Z^*(\omega_i)$ are impedance signatures (e.g., impedance magnitudes and real part and imaginary part of impedances) measured before and after damage for i th frequency, respectively; and N denotes the number of frequency points in the sweep. The RMSD equals to 0 if no damage. Otherwise, the RMSD is larger than 0. Due to experimental and environmental errors, however, the RMSD may be larger than 0 although damage is not occurred.

To deal with the uncertain conditions, the control chart analysis is used for decision-making out of the RMSD values. In this study, the upper control limit (UCL) is adopted for alarming damage occurrence, as follows

$$UCL_{RMSD} = \mu_{RMSD} + 3\sigma_{RMSD} \quad (8)$$

where μ_{RMSD} and σ_{RMSD} are mean and standard deviation of RMSDs, respectively. The occurrence of damage is indicated when the RMSD values are beyond (i.e., larger than) the bound of the UCL. Otherwise, there is no indication of damage occurrence.

2.3.2 Correlation coefficient of impedance signatures

Similar to the previous description, correlation coefficient of impedance signatures between before and after damage is computed as follows (Koo 2008)

$$\rho_{z, z^*} = \frac{E[Z(\omega)Z^*(\omega)] - \mu_z\mu_{z^*}}{\sigma_z\sigma_{z^*}} \quad (9)$$

where $Z(\omega)$ and $Z^*(\omega)$ are impedance signatures of a frequency band measured before and after damage, respectively. Also, μ_z and σ_z are mean and standard deviation values of impedance signals. Control chart analysis is used to alert damage occurrence from the correlation coefficients of impedance signatures. Lower control limit is determined similarly as described in Eq. (4).

3. Design of multi-scale sensor nodes

3.1 Hardware design of multi-scale sensor nodes

A multi-scale sensor node can be defined as a sensor node to simultaneously measure multiple physical quantities from structures in different scale. For the SHM using acceleration and impedance measurements, a multi-scale sensor node on Imote2 platform is designed as shown in Fig. 3. The Imote2 sensor platform was selected to control peripheral devices such as microcontroller, wireless radio and memory. For acceleration measurement, a SHM-A sensor board developed by Rice and Spencer (2008) was selected. For impedance measurement, an SSeL-I sensor board was newly designed in this study.

As shown in Fig. 4(a), the prototype of the multi-scale sensor node is consisted of four layers. The first and second layers are a battery board (IBB2400) and the Imote2 sensor platform (IPR2400), respectively. At present, Memsic Co. (2010) provides the Imote2 sensor platform and peripheral

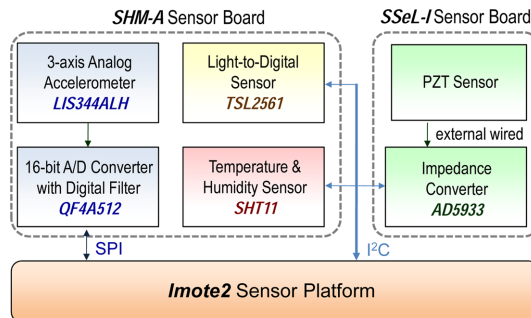
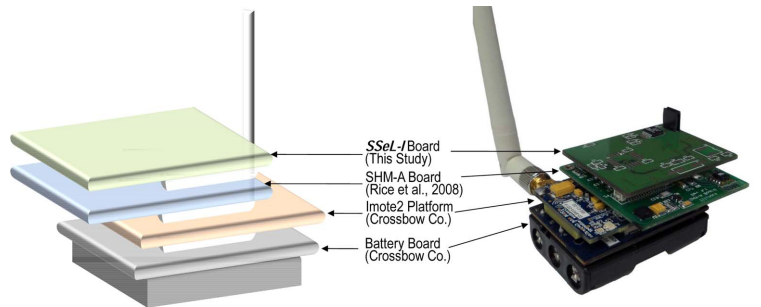
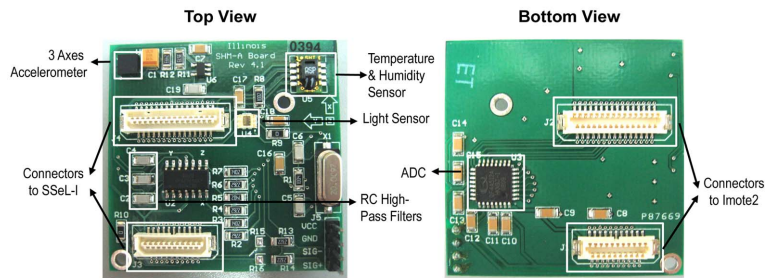


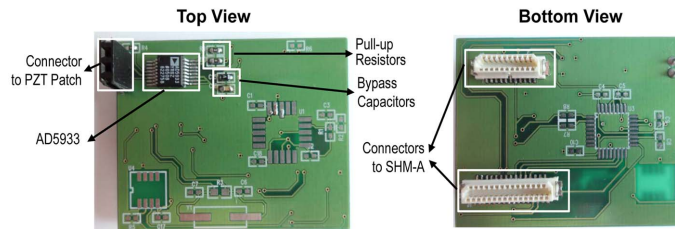
Fig. 3 Design of multi-scale sensor node for acceleration-impedance SHM



(a) Multi-layered sensor nodes on imote2 platform



(b) Acceleration sensor board: SHM-A



(c) Impedance sensor node: SSeL-I

Fig. 4 Multi-scale acceleration-impedance sensor nodes on Imote2 platform

devices associated with it. The third and fourth layers are the SHM-A acceleration sensor board and the SSeL-I impedance sensor board.

3.1.1 Imote2 sensor platform (Memsic Co., 2010)

For the acceleration-impedance sensor nodes, a sensor platform should be selected based on the capabilities of microcontroller, memory and wireless radio. As summarized in Table 1, the Imote2 has the high performance microcontroller and the large amount of data repository as compared to a smart sensor node (SSN) by Park *et al.* (2010). Firstly, the main board of the Imote2 incorporates a low-power X-scale process, PXA27x, and a wireless radio, CC2420. The microcontroller PXA27x runs for multiple tasks which include operation schedule, system control (e.g., AD5933 impedance chip and wireless radio), and radio transmission. It allows double-point precision valuables using 8 bytes. Note that a microcontroller ATmega128 used by Lynch *et al.* (2006) and Park *et al.* (2010) allows single precision floating point format using 4 bytes. Secondly, the Imote2 has 256 kB of integrated SRAM, 32 MB of external SDRAM, and 32 MB of program flash memory. The memory repository will guarantee to store large amount of data measured by a group of accelerometers and

Table 1 Comparison of sensor platforms: Imote2 by memsic co. (2010) Vs SSN by Park *et al.* (2010)

Feature	Imote2 by Memsic co. (2010)	SSN by Park <i>et al.</i> (2010)
Clock speed (MHz)	13-416	16
Active power (mW)	44 at 13 MHz 570 at 416 MHz	23 at 8 MHz 46 at 16 MHz
Program flash (bytes)	32 M	128 K
RAM	256 K + 32 M external	4 K + 32 K
Radio frequency (MHz)	2400	2400
Data rate (kbps)	250	250
Outdoor range (m)	30	100
Power of radio (mW)	52 when transmitting 59 when receiving 0.06 when powered-down	149 when transmitting 165 when receiving 0.03 when powered-down

PZT patches. Thirdly, although the Imote2 consumes more power in high-speed mode and the embedded wireless radio has short transmitting distance, the data processing speed of the Imote2 is faster enough to provide good computational capability and the transmitting distance can be expanded up to 125 m by using an external antenna. Based on the above-mentioned performances, the Imote2 sensor platform is selected for the hybrid acceleration-impedance-based SHM.

3.1.2 SHM-A sensor board for acceleration measurement (Rice and Spencer, 2008)

As shown in Fig. 4(b), the SHM-A sensor board developed by Rice and Spencer (2008) was selected for acceleration measurement. Commercialized SHM-A (ISM400) boards are available from Memsic Co (2010). As outlined in Table 2, the SHM-A sensor board was compared with a wired ICP-type accelerometer PCB393B04 and the corresponding signal conditioner PCB481A03 (which are used for the performance evaluation of the multiscale sensor node). Compared to the wired PCB system, the wireless SHM-A sensor board has relatively low sensitivity and relative high noise density. But its cost along with the use of the Imote2 sensor platform is much lower than the conventional wired measurement system.

For the acceleration measurement, the SHM-A sensor board should have suitable capabilities for key components such as accelerometer, noise density, anti-aliasing filter, and analog-to-digital converter (ADC). The sensor board provides three-axes-acceleration sensor (LIS344ALH) with relative low noise

Table 2 Comparison of acceleration measurement systems: Wired PCB Vs Wireless SHM-A

Hardware	Feature	Wireless system SHM-A	Wired system PCB
	Model	LIS344ALH	PCB393B04
Accelerometer	Sensitivity (mV/g)	660	1000
	Measurable range (g)	±2	±5
	Bandwidth (kHz)	1.5	2
	Noise floor ($\mu V/\sqrt{Hz}$)	50	0.3
Data acquisition	Model	QF4A512	NI6036E
	ADC resolution (bits)	16	16
Signal conditioner	Model	QF4A512	PCB481A03
	Filter type	Digital filter	Digital filter

level, light sensor (TSL2561), temperature and humidity measurements (SHT11). Also, the 4-channel 16-bit high resolution analog-to-digital converter (ADC) with digital anti-aliasing filters (QF4A512) is adopted. The ADC converts analog signal to digital data by 16 bit resolution but it guarantees 12 bit resolution. By adopting the digital filters, the sensor board provides user-selectable anti-aliasing filters and sample rates that can meet a wide range of application demands for infrastructure monitoring (Rice and Spencer 2008).

3.1.3 SSeL-I sensor board for impedance measurement

As shown in Fig. 4(c), the SSeL-I sensor board was newly developed in this study for impedance-based SHM. Similar to the one presented by Mascarenas *et al.* (2007) and Park *et al.* (2010), the SSeL-I sensor board was designed as schematized in Fig. 5. On Imote2-platform, the SSeL-I is consisted of an impedance converter AD5933, two pull-up resistors for I²C communication, two capacitors for bypassing noises, a connector to a PZT patch and two connectors to the SHM-A sensor board and the Imote2 sensor platform.

Two pull-up resistors are utilized for I²C interface communication between the SSeL-I board and the Imote2 platform. The microcontroller PXA27x and wireless radio CC2420 in the Imote2 platform are utilized for the impedance measurement. The AD5933 impedance converter has the following embedded multi-functional circuits: function generator, digital-to-analog (D/A) converter, current-to-voltage amplifier, anti-aliasing filter, A/D converter, and discrete Fourier transform (DFT) analyzer. The AD5933 converter outputs real and imaginary values of impedance signatures for a target frequency of interest and transmits the values into a microcontroller.

As summarized in Table 3, the specification of the developed SSeL-I sensor board is compared with one of a commercial impedance analyzer HIOKI3532. The measurable range of the wireless SSeL-I sensor board is much smaller than that of the wired HIOKI impedance analyzer. The disadvantage may interfere with wide applications of the SSeL-I sensor board into real structures. To overcome the disadvantage, in this study, an interface washer proposed by Park *et al.* (2010) is employed as a complement device for high-sensitivity and fixed-range impedance measurement by the SSeL-I sensor board. By using the interface washer, it may provide the following benefits (Park *et al.* 2010): 1)

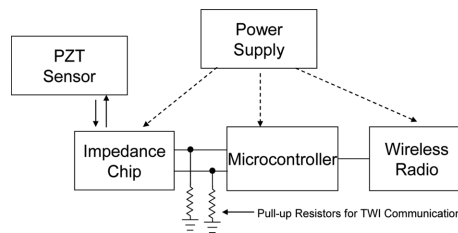


Fig. 5 Schematic of impedance-based smart sensor Node: SSeL-I board

Table 3 Comparison of impedance measurement systems: Wired HIOKI Vs Wireless SSeL-I

Hardware	Feature	Wireless system SSeL-I	Wired system HIOKI
Impedance analyzer	Model	AD5933	HIOKI3532
	Impedance Range	1 kΩ - 10 kΩ	10 kΩ - 200 kΩ
	Frequency Range	1 kHz - 100 kHz	42 Hz - 5 MHz
	Excitation Voltage	1.98 V_{p-p}	14 V_{p-p}
PZT patch	Model	PZT 5A	PZT 5A

sensitive impedance features to the change in structural system and 2) relatively constant frequency range independent of target structures.

3.2 Software design of multi-scale sensor nodes

To operate the multi-scale sensor nodes ‘*Imote2/SHM-A/SSeL-I*’, device drivers (specified in Fig. 3) are programmed as Fig. 6, according to UIUC ISHMP (Illinois Structural Health Monitoring Project, 2010) Service Toolsuite and PKNU SSeL (Smart Structure engineering Lab) SHM tools (Park *et al.* 2010). The ISHMP Service Toolsuite provides an opensource software library of customized services such as device drivers and mathematical functions for SHM applications. The ISHMP Services Toolsuite and the SSeL SHM tools on the Imote2 employs TinyOS which is a lightweight operating system specifically designed for low-power wireless sensors. TinyOS applications are easily programmed by wiring components (Levis and Gay 2009).

For synchronized acceleration measurements, a ‘*RemoteSensing*’ component from ISHMP Services Toolsuite is used for the SHM-A sensor boards (SHM-A User Guide, 2010). After all leaf nodes located on a structure finish acceleration measurements, each leaf node transmits the measured data to a base station as shown in Fig. 6. Then the base station is programmed by SSeL SHM tools. For the SHM-A sensor boards, the SSeL SHM tools include a device driver for ADC and mathematical functions for damage monitoring such as PSD, CC of PSD, and MSE-based damage index (Eq. (1) - Eq. (6)). Also, the frequency domain decomposition (FDD) method (Brincker *et al.* 2001, Yi and Yun 2004) is embedded into the system to extract modal parameters such as natural frequencies and mode shapes.

For the impedance measurements from the SSeL-I impedance sensor board, an ‘*I2CControl*’ component provided from ISHMP Services Toolsuite and an ‘*Impedance*’ component (i.e., the device driver to operate AD5933) programmed by SSeL SHM tools as shown in Fig. 6. Each leaf node measures impedance signals and transmits the measured data to the base station. Then the base station performs the impedance-based damage detection. For the SSeL-I impedance sensor board, the SSeL SHM tools include a device driver for impedance components and mathematical functions for damage monitoring such as CC and RMSD (Eq. (7) - Eq. (9)).

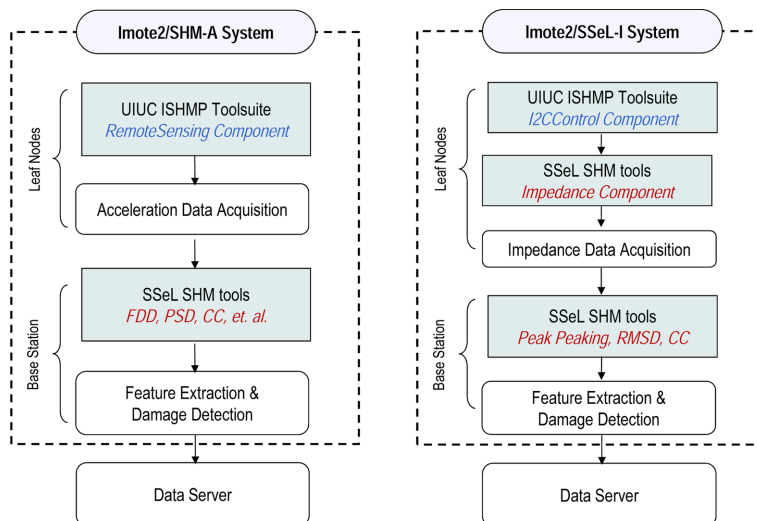


Fig. 6 Schematic of embedded software in multi-scale sensor nodes

3.2.1 Software for Imote2/SHM-A

As schematized in Fig. 7, the acceleration-based damage monitoring procedure was designed to be embedded in the wireless Imote2/SHM-A system. The vibration-based damage monitoring algorithm consists of three phases: ‘Initialization’, ‘Alarming’, and ‘Localization’. The software for the procedure was programmed by TinyOS.

In Phase 1, the statistical criterion of damage alarming for the target structure is determined. Firstly, each sensor node measures accelerations from the ADC. If $k = 0$ ($k = 0, 1, 2, \dots, m$, where m is the number of measurements). A base station node receives acceleration data measured from the other-sensor nodes. Secondly, natural frequencies and mode-shapes are extracted by computing PSD (Eq. (1)) and the FDD method (Brincker *et al.* 2001, Yi and Yun 2004). The extracted data are stored in the memory and utilized as references (e.g., PSD_0 in Fig. 7) to calculate the CC of PSDs (Eq. (3)). Thirdly, the sensor node repeats measurements and calculates the CCs between the reference PSD_0 and each measured PSD_k until k equals m . Finally, the sensor node determines a lower control limit (LCL) by Eq. (4).

In Phase 2, the occurrence of damage is alerted by the damage alarming criteria. Firstly, the sensor node measures acceleration from the ADC and calculates PSD_n . Secondly, a CC of PSDs is calculated by using PSD_n and PSD_0 stored in the memory. Finally, damage is alarmed if the CC is beyond the bound of the LCL. If the damage is alarmed, the location of damage is estimated by Phase 3.

In Phase 3, the location of damage is estimated in the damage-alerted structural system. First, the sensor node receives acceleration data from the other sensors and extracts modal parameters. Then, modal strain-energies for the present and the reference mode-shapes are calculated and the damage location is predicted by the MSE-based damage index (Eqs. (5) and (6)).

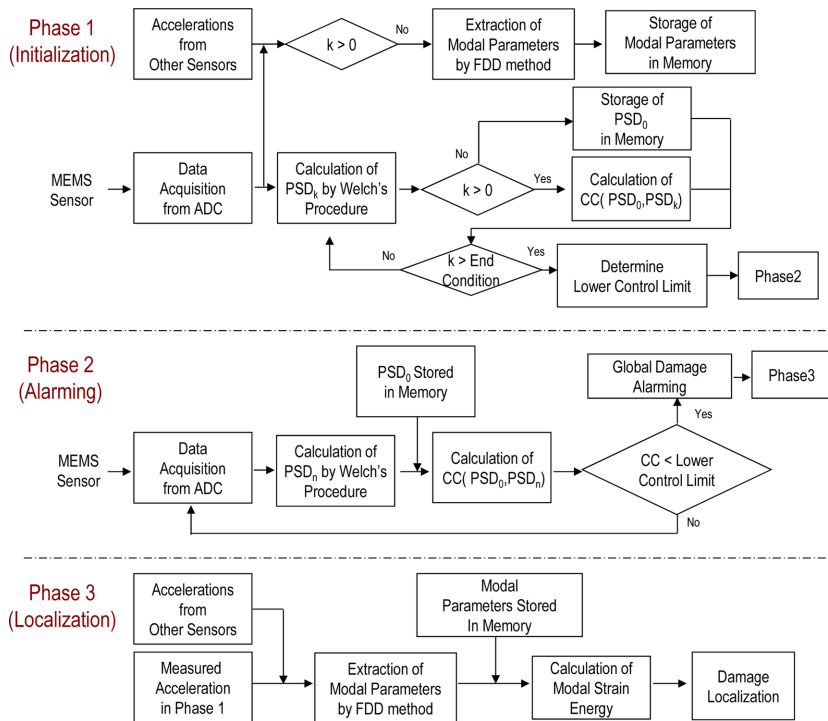


Fig. 7 Schematic of acceleration-based monitoring procedure for Imote2/SHM-A

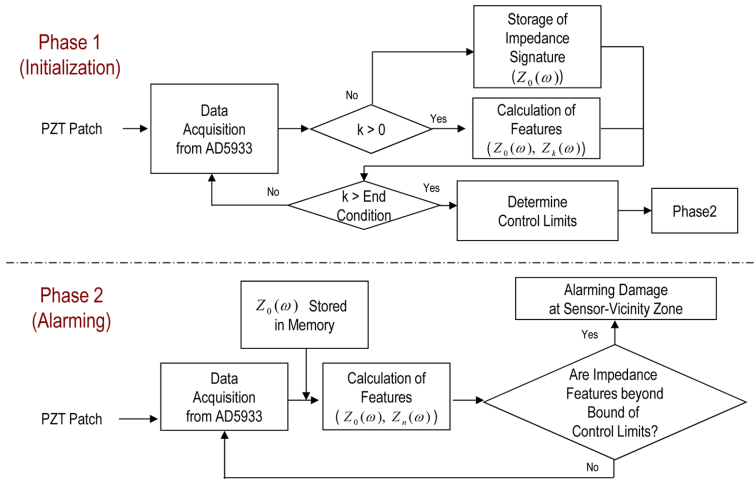


Fig. 8 Schematic of impedance-based monitoring procedure for Imote2/SSeL-I

3.2.2 Software for Imote2/SSeL-I

As schematized in Fig. 8, the impedance-based damage monitoring procedure was designed to be embedded in Imote2/SSeL-I. The impedance-based damage monitoring algorithm consisted of two phases: ‘Initialization’ and ‘Alarming’. The software for the procedure was also programmed by TinyOS.

In Phase 1, the criterion of damage alarming is determined from stochastic process for the target structural member. Firstly, the SSeL-I sensor node measures impedance signatures from the impedance converter AD5933. Secondly, if $k = 0$, the impedance signature $Z_0(\omega)$ are stored in the memory. The stored data is utilized as references to calculate the CC and the RMSD of impedance signatures by Eqs. (7) and (9). Thirdly, the sensor node repeats measurements and calculates the CCs between the reference $Z_0(\omega)$ and each measured impedance signatures $Z_k(\omega)$ until k equals m . Finally, the sensor node determines control limits as defined in Eqs. (4) and (8).

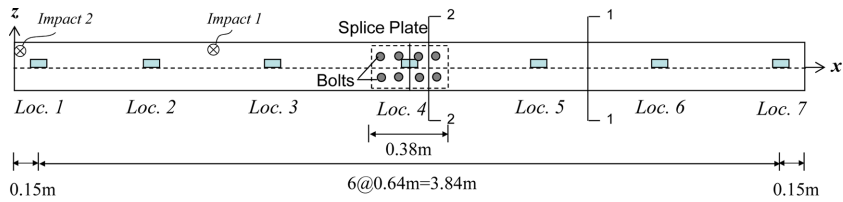
In Phase 2, the occurrence of damage is alerted by the damage alarming criteria. Firstly, the sensor node measures impedance signature $Z_n(\omega)$ from AD5933. Secondly, CC and RMSD values are calculated by using $Z_n(\omega)$ and $Z_0(\omega)$ stored in the memory. Finally, if the CC and RMSD values are beyond bound of the control limits, it indicates that the damage is alarmed at the sensor-vicinity zone.

4. Performance evaluation of multi-scale sensor nodes

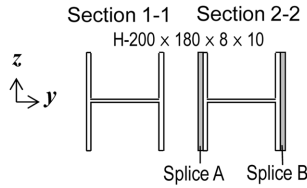
4.1 Test structure and experimental setup

A lab-scaled steel girder model with bolted connections was used to evaluate the performance of the multiscale sensor nodes. As shown in Figs. 9 and 10, the girder is H-section ($H-200 \times 180 \times 8 \times 100$), 4.14 m span-length, and free-free boundary condition. As shown in the figures, two girder sections (2.07 m length each) are connected by splice plates and bolts on the flanges.

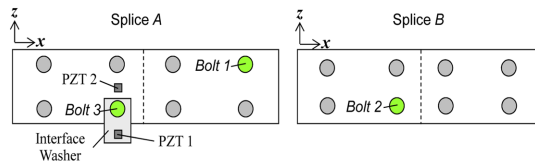
For acceleration monitoring, the Imote2/SHM-A sensor nodes were installed on the test girder to measure vibrations in y-direction. Locations and arrangements of the sensor nodes were designed as



(a) Girder dimension and sensor layout



(b) Cross section



(c) Splice plates

Fig. 9 Schematic of bolt-connected steel girder

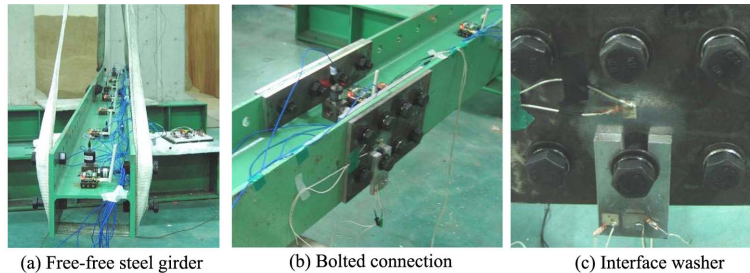


Fig. 10 Experimental setup of bolt-connected steel girder

shown in Fig. 9. Seven Imote2/SHM-A sensor nodes (Loc. 1-7) were placed on the web of the girder with constant interval of 0.64 m. Also, seven wired PCB393B04 accelerometers (as described in Table 2) were also mounted on the girder at the corresponding points. The wired data acquisition system includes the 16-channel PCB481A03 signal conditioner, the 16-channel 16-bit DAQ card and a laptop with MATLAB. As marked in Fig. 9, an impact excitation point (Impact 1) was selected at a location distanced 1m from the left edge between Loc. 2 and Loc. 3. The impact was applied on the right flange (i.e., y-direction) by an impact hammer.

As shown in Figs. 9(c) and 10(c), an interface washer was installed for high-sensitivity and fixed frequency range of impedance measurement. It was placed between the splice plate and Bolt 3. One edge of the interface washer was fixed by the connection bolts, but the other end was free boundary condition. A PZT patch (PZT 1) was placed on the interface washer. Also, another PZT patch (PZT 2) was placed directly on the splice plate (i.e., Splice A). Both PZT 1 and PZT 2 were 10 mm×10 mm and PZT 5A type. The PZT patches were connected to an Imote/SSeL-I sensor node at Loc. 4. The

Table 4 Damage scenarios inflicted in bolt-connected steel girder

Damage case	Damage scenario
Reference	All bolts fastened by 160 N-m
Bolt1	Bolt 1 loosened by 35 N-m, all others remained as 160 N-m
Bolt2	Bolt 2 loosened by 35 N-m, all others remained as 160 N-m
Bolt3	Bolt 3 loosened by 35 N-m, all others remained as 160 N-m

impedance signatures were also measured by the commercial impedance analyzer HIOKI 3532 and those data were used for the performance evaluation of the multi-scale sensor node. The input voltage into the PZT patches was set up to $1.98 V_{p-p}$ which is the maximum output voltage from AD5933 in the SSeL-I sensor board. The same input voltage was also set for the commercial impedance analyzer HIOKI 3532.

Table 4 shows damage scenarios for bolt-loosening of the girder. The damage scenarios include one reference and three bolt-loosening damage cases. The reference case is that all bolts are fastened by torque of 160 N-m. The three damage cases are that each bolt (i.e., Bolt 1, 2 or 3) is loosened to torque of 35 Nm. Bolt 3 on the Splice A is arbitrarily selected among the nearest four bolts from the center of the girder at which the two beams are connected. Bolt 1 is the most distanced (i.e., 17.2 cm) from Bolt 3 among eight bolts on Splice A. Bolt 2 is located on the opposite splice plate (i.e., Splice B). During the experiments, temperature and humidity were kept almost constant as 18-degree Celsius and 35 percent, respectively, by air-conditioners.

4.2 Evaluation of multi-scale sensor nodes (Imote2/SHM-A/SSeL-I)

The performances of the multi-scale sensor nodes were evaluated by comparing with commercial measurement systems in two aspects as: 1) vibration measurement and feature extraction and 2) impedance measurement and feature extraction.

4.2.1 Vibration measurement and feature extraction

Both the Imote2/SHM-A sensor node and the wired PCB system were used to measure acceleration responses of the girder model from impact hammer tests. The impact excitation was applied to the girder between Loc. 2 and Loc. 3. Signals were obtained for 12 seconds with sampling frequency of 1 kHz and low-pass filter of 250 Hz. Fig. 11(a) shows the time-domain acceleration-responses measured at Loc. 3 from the wireless Imote2/SHM-A and the wired PCB393B04. It is noted that the acceleration intensities are a little different each other. Fig. 11(b) shows the frequency-domain responses of the wireless Imote2/SHM-A and the wired PCB393B04. The power spectral densities are good matched each other. It is also observed that the power spectral densities have two major peaks around 80 Hz and 210 Hz which are corresponding to the first two bending modes.

To extract natural frequencies and mode-shapes, the frequency domain decomposition method was employed (Brincker *et al.* 2001, Yi and Yun 2004). As shown in Fig. 12(a) and also listed in Table 5, natural frequencies and mode-shapes of the first two modes of the girder were measured from the wireless Imote2/SHM-A and the wired PCB system. They are not good matches in the first and second modes. The differences in natural frequencies and mode shapes may be attributed to the choice of MEMS accelerometer in the SHM-A sensor board. As listed in Table 2, the MEMS accelerometer (LIS344ALH) has relatively low sensitivity and high noise level. Also, the impact

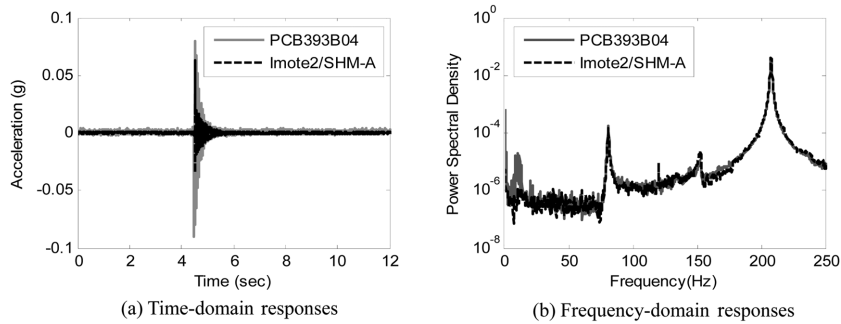


Fig. 11 Acceleration responses of bolt-connected steel girder: wired PCB system Vs wireless Imote2/SHM-A system

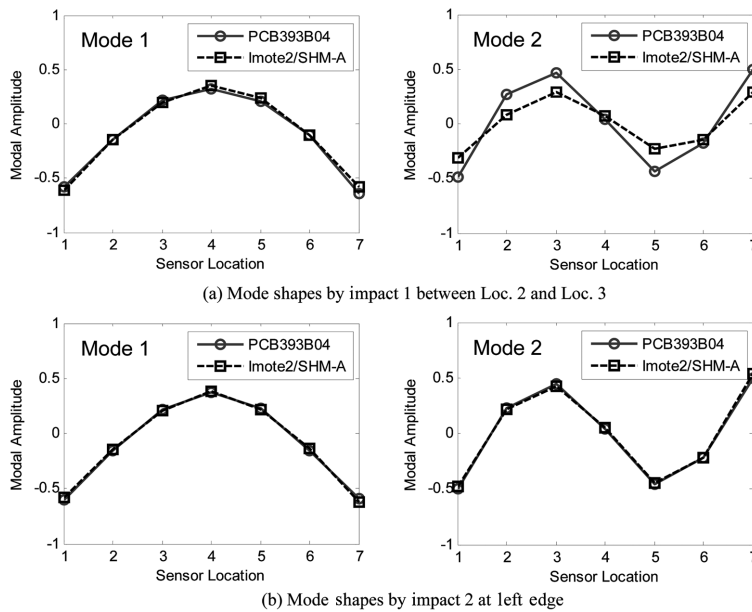


Fig. 12 Experimental mode-shapes of bolt-connected steel girder: Wired PCB System Vs Wireless Imote2/SHM-A System

location affects the acceleration intensity due to exciting nearby a node of mode.

To examine the effect of the acceleration intensity on the accuracy of the mode-shapes, an additional test was performed by selecting another impact location (Impact 2) as the left edge of the girder at which the acceleration intensity would be increased. As shown in Fig. 12(b), both the first and second mode-shapes from the wireless Imote2/SHM-A system and the wired PCB system are good matched with small errors.

4.2.2 Impedance measurement and feature extraction

Impedance responses between 10 kHz and 100 kHz were measured from PZT 1 on the interface washer by Imote2 and SSeL-I (Imote2/SSeL-I) of the multi-scale sensor node and the impedance analyzer HIOKI3532. As Analog Devices (2010) recommended, two-point calibration was used to increase the accuracy of the measured impedance magnitude and phase. Fig. 13 shows the measured

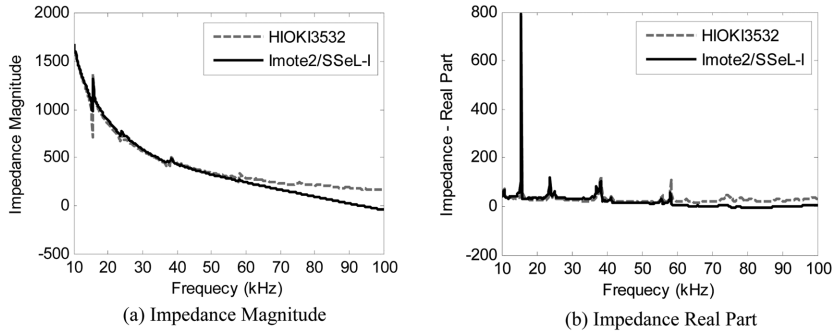


Fig. 13 Impedance signatures by PZT 1 on interface washer: wired HIOKI system Vs wireless Imote2/SSeL-I system

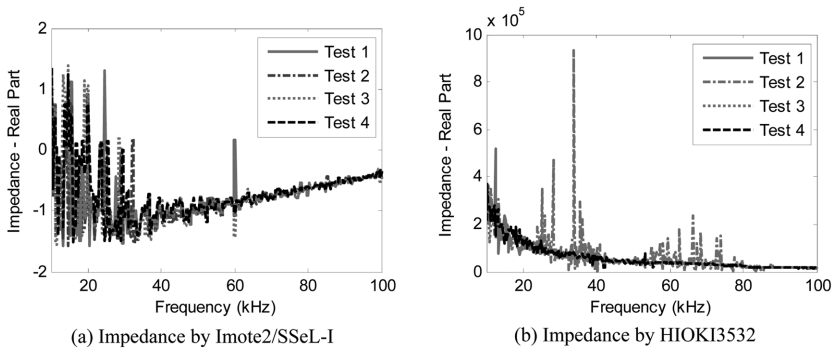


Fig. 14 Impedance signatures by PZT 2 on steel girder: wired HIOKI system Vs wireless Imote2/SSeL-I system

impedance magnitude and the real part of the impedance from PZT 1 on the interface washer by Imote2/SSeL-I and HIOKI3532. As shown in Fig. 13, the impedances in a range over 15 kHz are beyond the minimum measurable impedance (i.e., $1\text{ k}\Omega$) of AD5933, as listed in Table 3. The impedance signatures measured by Imote2/SSeL-I are good matched to those by HIOKI3532 in a range less than 60 kHz.

To validate the feasibility of the interface washer, the impedance signatures measured by using the interface washer was experimentally compared to those measured directly from the structure. As shown in Fig. 14, impedance signatures between 10 kHz and 100 kHz were directly measured from PZT 2 on Splice A. For the wireless Imote2/SSeL-I system and the wired HIOKI system, the impedance signatures were repeatedly measured from four ensemble tests of the same condition. However, no meaningful repeatable peak point is found in the impedance signatures between 10 kHz and 100 kHz. That is, all peaks in the impedance signatures can be considered as those due to noise.

4.3 Damage monitoring by multi-scale sensor nodes (Imote2/SHM-A/SSeL-I)

As listed in Table 4, a set of damage cases were introduced into the girder by bolt-loosening. Then damage monitoring in test structure was performed in two phases: (1) global vibration-based damage monitoring by Imote2/SHM-A and (2) local impedance-based damage monitoring by Imote2/SSeL-I.

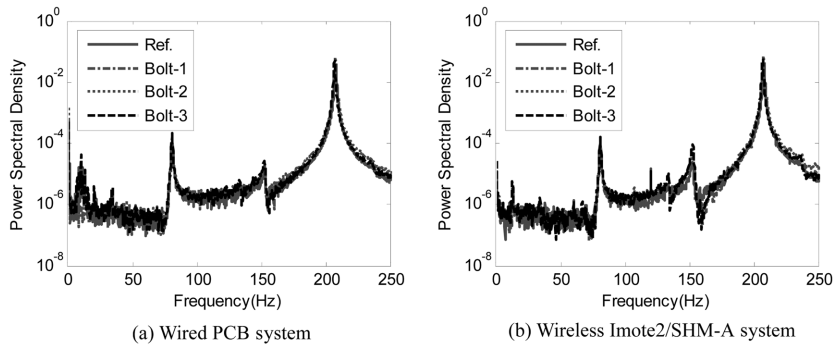


Fig. 15 Power spectral densities (PSDs) for bolt-loosening damage cases

4.3.1 Global vibration-based damage monitoring by Imote2/SHM-A

Global vibration-based damage monitoring in the girder connection was performed in three steps: damage-occurrence alarming, modal parameter identification, and MSE-based damage estimation. For comparison, the global monitoring results were presented for the wired PCB system and the wireless Imote2/SHM-A system, one another.

Firstly, the occurrence of damage was monitored in a global manner by using the cross-correlation of PSDs of Eq. (1). For the undamaged and three damage states, acceleration signals up to four ensembles were measured from Loc. 3 sensor. For each ensemble, acceleration responses were acquired for 15 seconds under several impact forces. For the undamaged and three damaged cases, as shown in Figs. 15(a) and (b), power spectral densities were computed for the acceleration responses measured from the wired PCB system and the wireless Imote2/SHM-A system. For the undamaged reference state and also for the bolt loosening damage cases, as shown in Figs. 16(a) and (b), the correlation coefficients of PSDs were obtained for the acceleration responses measured from the wired PCB system and the wireless Imote2/SHM-A system. Four ensembles of the undamaged state were used to decide a lower control limit (LCL) for damage alarming. All damage cases were successfully alerted both by the wired system and the wireless system. Note that the correlation coefficient values in Fig. 16(b) have relatively large variations which may be caused by high density noises in the acceleration signals of the Imote2/SHM-A sensor nodes as shown in Fig. 11(a).

Secondly, modal parameters were extracted from acceleration signals measured at the seven sensor locations (i.e., Loc. 1 - Loc. 7) by using the embedded FDD method. For the undamaged and three

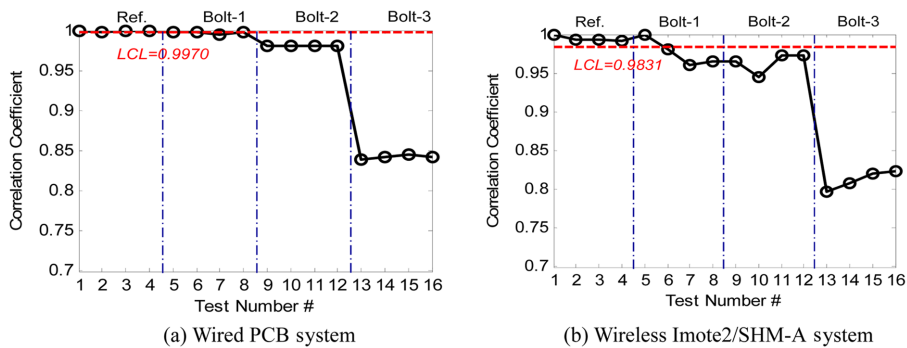


Fig. 16 Correlation coefficients of PSDs for bolt-loosening damage cases

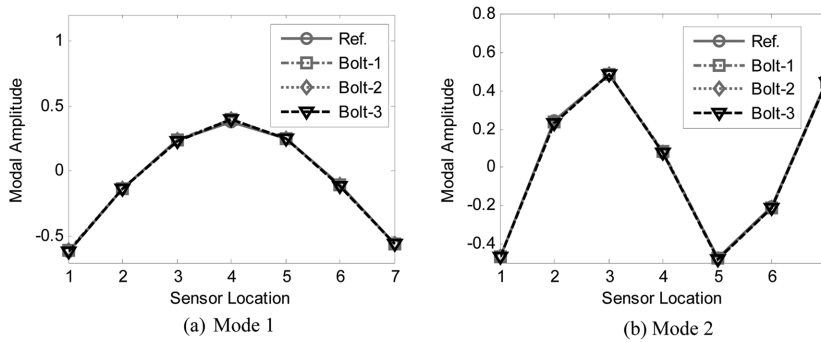


Fig. 17 Experimental mode shapes for bolt-loosening damage cases: wired PCB system

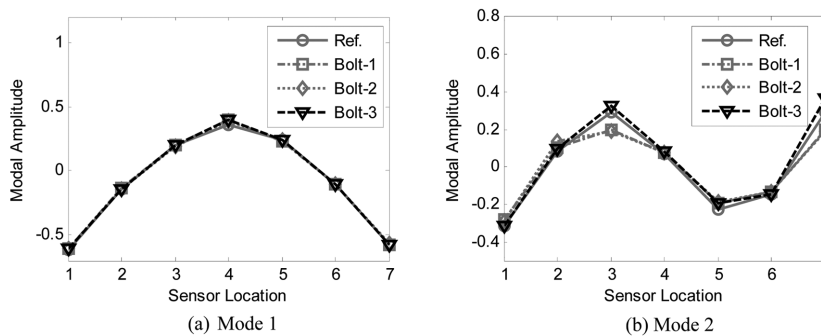


Fig. 18 Experimental mode shapes for bolt-loosening damage cases: wireless Imote2/SHM-A system

Table 5 Natural frequencies for undamaged and bolt loosening damage cases

Damage case	Wired PCB system		Wireless Imote2/SHM-A system	
	Mode 1 (Hz)	Mode 2 (Hz)	Mode 1 (Hz)	Mode 2 (Hz)
Reference	80.93	208.66	80.93	208.73
Bolt1	80.93	208.62	80.93	208.62
Bolt2	80.81	208.40	80.93	208.40
Bolt3	80.93	208.01	80.88	208.15

damaged cases, the first two bending mode shapes were measured from the wired PCB393B04 accelerometers as shown in Fig. 17 and also measured from the wireless Imote2/SHM-A sensor nodes as shown in Fig. 18. The corresponding natural frequencies measured by the two systems are listed in Table 5. Next, mode shapes were post-processed by ten (10) pseudo-readings in-between two adjacent sensors by using cubic-spline interpolation functions (See Kim *et al.* (2003) for details). Then modal curvatures were analyzed from the post-processed mode shapes, from which modal strain energies of girder elements were computed as defined in Eq. (5). For the undamaged and three damage states, as shown in Figs. 19 and 20, modal strain energies of the first two modes were extracted from the wired PCB system and the wireless Imote2/SHM-A system, respectively.

Finally, the MSE-based damage index method was utilized for detailed damage estimation. The damage location index, β_j , was computed according to Eq. (5). As shown in Figs. 21 and 22, the

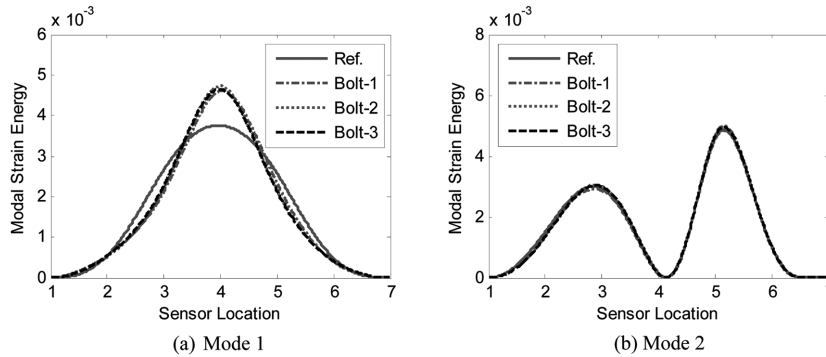


Fig. 19 Modal strain energies extracted for bolt-loosening damage cases: wired PCB system

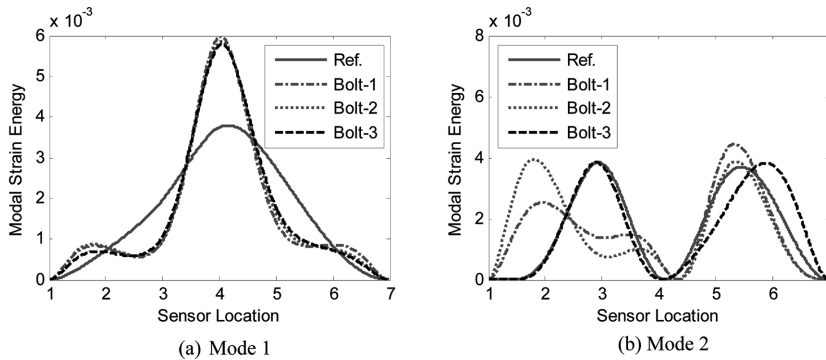


Fig. 20 Modal strain energies extracted for bolt-loosening damage cases: wireless Imote2/SHM-A system

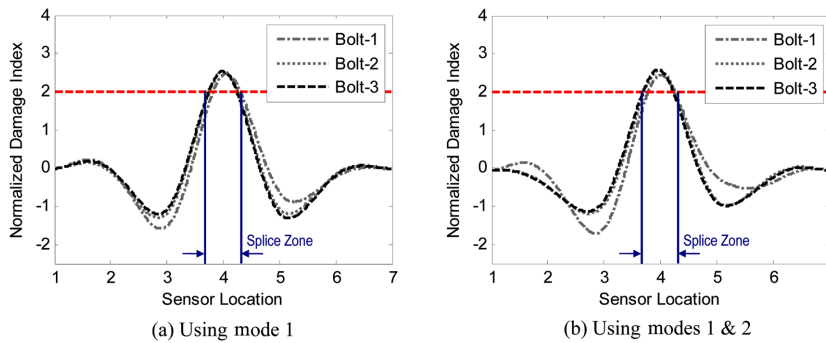


Fig. 21 MSE-based damage location indices for bolt-loosening damage cases: wired PCB system

normalized damage indices were computed for the wired PCB system and the wireless Imote2/SHM-A system, respectively. In assigning damage to a particular location, the decision rule of Eq. (6) was utilized. In both figures, the dotlines are the objective threshold with confidence level of 97.2%. For the wired PCB system, damage locations were correctly predicted both by using mode 1 (Fig. 21(a)) and by using modes 1 and 2 (Fig. 21(b)). For the wireless Imote2/SHM-A system, damage locations were correctly predicted by using mode 1 (Fig. 22(a)) but incorrectly estimated by using modes 1 and 2 (Fig. 22(b)).

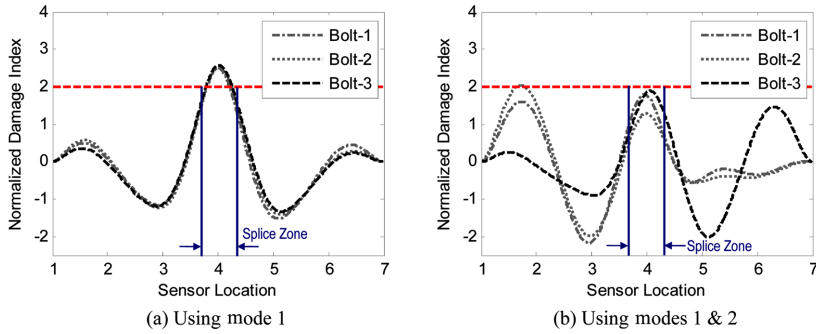


Fig. 22 MSE-based damage location indices for bolt-loosening damage cases: wireless Imote2/SHM-A system

4.3.2 Local impedance-based damage monitoring by Imote2/SSeL-I

The occurrence of damage was monitoring from PZT 1 impedance patch on the interface washer. The monitoring results were presented for the wired HIOKI system and the wireless Imote2/SSeL-I system. As shown in Fig. 23, the impedance signatures were measured for the bolt loosening damage cases. Then the RMSDs and correlation coefficients were calculated by Eqs. (7) - (9). Fig. 24 shows the damage alarming results by using the RMSD of impedance signatures. Also, Fig. 25 shows the results by using the correlation coefficients of impedance signatures. In those figures, the dotlines are upper control limits (UCL) for damage alarming by using the RMSD and lower control limits

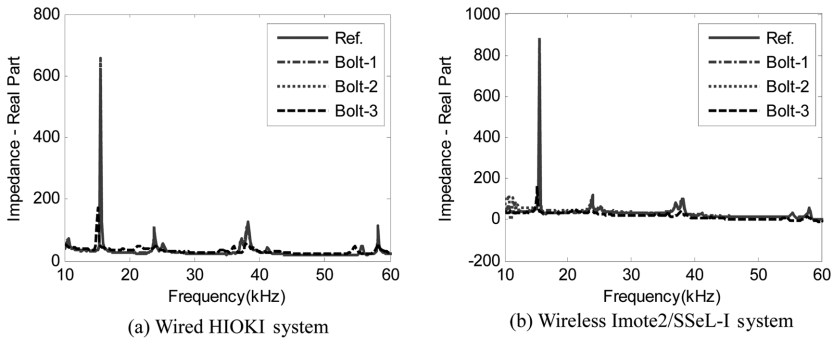


Fig. 23 Impedance signatures for bolt loosening damage cases

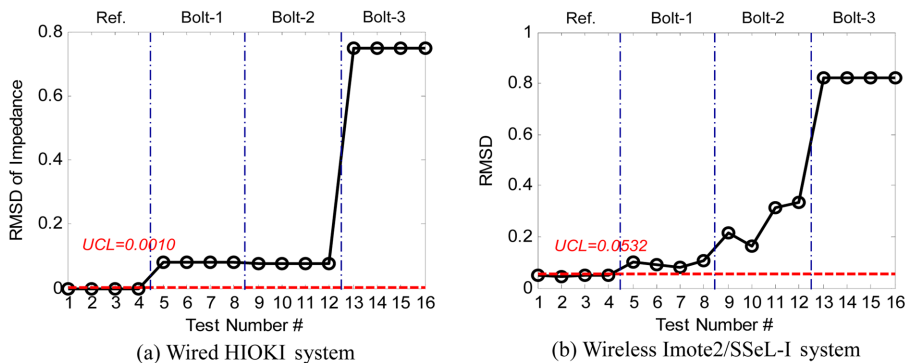


Fig. 24 RMSDs of impedance signatures for bolt loosening damage cases

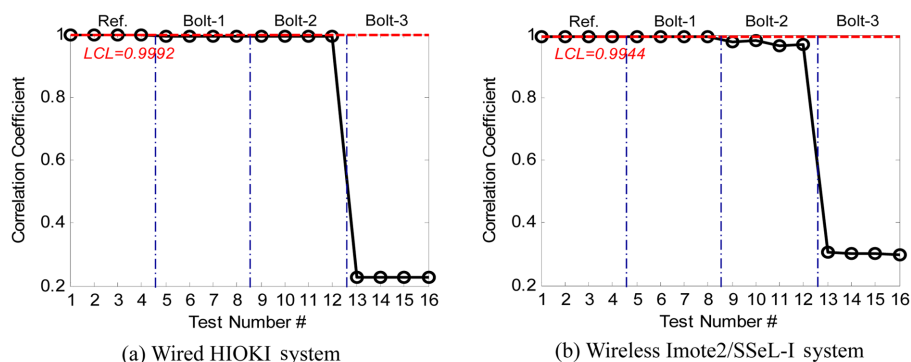


Fig. 25 Correlation coefficients of impedance signatures for bolt loosening damage cases

(LCL) by using the correlation coefficients.

By the RMSD values in Fig. 24, both the wired HIOKI system and the wireless Imote2/SSeL-I system were successful to alert all bolt-loosening damages. By the correlation coefficient values in Fig. 25, however, both the wired system and the wireless system were successful only to alert Bolt-3 damage case. Note also that the wireless Imote2/SSeL-I system produced relatively large variations in the RMSD values.

5. Conclusions

In this study, hybrid acceleration-impedance sensor nodes on Imote2-platform were designed for damage monitoring in steel structural connections. Thus, the feasibility of the sensor nodes was examined about its performance for vibration-based global monitoring and impedance-based local monitoring in the structural systems. To achieve the objective, the following approaches were implemented. Firstly, a damage monitoring scheme was described in parallel with global vibration-based methods and local impedance-based methods. Secondly, multi-scale sensor nodes were designed for acceleration-impedance monitoring process by combining Imote2 sensor platform, SHM-A acceleration sensor board, and SSeL-I impedance sensor board. Also, the software was designed to operate the multi-scale sensor nodes, and to perform local impedance-based damage monitoring and global vibration-based damage monitoring. Thirdly, the performance of the multi-scale sensor nodes was experimentally evaluated from damage monitoring in a lab-scaled steel girder with bolted connection joints.

From the evaluation experiments, the following conclusions have been made. Firstly, the acceleration responses, the power spectral densities, and the mode shapes were accurately measured from the wireless Imote2/SHM-A acceleration system, as compared to the wired PCB acceleration system. For global vibration-based damage monitoring, the wireless Imote2/SHM-A system successfully alerted all bolt-loosening damage cases by using the correlation coefficient of power spectral densities which were measured before and after a damaging event. Also, the damage locations were correctly predicted by using the modal strain energy-based damage index method. Secondly, the impedance signatures were accurately measured from the wireless Imote2/SSeL-I impedance system, as compared to the wired HIOKI impedance system. For local impedance-based damage monitoring, the wireless Imote2/SSeL-I system successfully alerted all bolt-loosening damage cases.

This study was focused on evaluating the performance of the designed hybrid sensor node on Imote2 platform in the lab-scaled steel girder. Future research remains to improve the multi-scale sensor node for field application by dealing with temperature-induced uncertainty and power management problem. Also, research efforts are needed to improve the hybrid damage monitoring algorithm using acceleration and impedance signatures and the interface washer for the improvement of reliability and practicality of monitoring results in real structures.

Acknowledgements

This work was supported by the Korea Research Foundation Grant funded by the Korean Government (MOEHRD, Basic Research Promotion Fund) (KRF-2008-314-D00414), and the student involved in this research was supported by the Brain Korea 21 program granted by Ministry of Education, Science and Technology of Korea.

References

- Analog Devices (2010), “*Datasheet of AD5933*”, Available from <<http://www.analog.com>>.
- Bendat, J.S. and Piersol, A.G. (2003), “*Engineering applications of correlation and spectral analysis*”, Wiley-Interscience, New York, NY.
- Bhalla, S. and Soh, C.K. (2004), “Structural health monitoring by piezo-impedance transducers ii: applications”, *J. Aerospace. Eng.*, **17**(4), 166-175.
- Brincker, R., Zhang, L. and Andersen, P. (2001), “Modal identification of output-only systems using frequency domain decomposition”, *Smart Mater. Struct.*, **10**(3), 441-445.
- Cho, S., Yun, C.B., Lynch, J.P., Zimmerman, A.T., Spencer, B.F. and Nagayama, T. (2008), “Smart wireless sensor technology for structural health monitoring of civil structures”, *Steel Struct.*, **8**, 267-275.
- Fasel, T.R., Sohn, H., Park, G. and Farrar, C.R. (2005), “Active sensing using impedancebased ARX models and extreme value statistics for damage detection”, *Earthq. Eng. Struct. D.*, **34**(7), 763-785.
- Giurgiutiu, V. and Zagari, A.N. (2002), “Embedded self-sensing piezoelectric active sensors for on-line structural identification”, *J. Vib. Acoust.*, **124**(1), 116-125.
- Illinois Structural Health Monitoring Project (2010), Available from: <<http://shm.cs.uiuc.edu/>>
- Kim, J.T. and Stubbs, N. (1995), “Model uncertainty impact and damage-detection accuracy in plate girder”, *J. Struct. Eng.*, **121**(10), 1409-1417.
- Kim, J.T., Ryu, Y.S., Cho, H.M. and Stubbs, N. (2003), “Damage identification in beamtype structures: frequencybased method vs modeshapebased method”, *Eng. Struct.*, **25**(1), 57-67.
- Kim, J.T., Na, W.B., Hong, D.S. and Park, J.H. (2006a), “Global and local health monitoring of plate-girder bridges under uncertain temperature conditions”, *Steel Struct.*, **6**, 369-376.
- Kim, J.T., Na, W.B., Park, J.H. and Hong, D.S. (2006b), “Hybrid health monitoring of structural joints using modal parameters and EMI signatures”, *Proceedings of the SPIE*. 6174, San Diego.
- Kim, J.T., Park, J.H., Hong, D.S., Cho, H.M., Na, W.B. and Yi, J.H. (2009), “Vibration and impedance monitoring for prestressloss prediction in PSC girder bridges”, *Smart Struct. Syst.*, **5**(1), 81-94.
- Koo, K.Y. (2008), “*Structural health monitoring methods for bridges using ambient vibration and impedance measurements*”, Ph.D. Dissertation, Korea Advanced Institute of Science and Technology, Daejeon, Korea.
- Krishnamurthy, V., Fowler, K. and Sazonov, E. (2008), “The effect of time synchronization of wireless sensors on the modal analysis of structures”, *Smart Mater. Struct.*, **17**(5), 1-13.
- Kurata, N., Spencer, B.F. and RuizSandoval M. (2005), “Risk monitoring of buildings with wireless sensor networks”, *Struct. Control Health Monit.*, **12**(3-4), 315-327.
- Kyung, G.S., Lee, J.S., Choi, I.Y. and Hong, S.U. (2002), “Classification and analysis: deteriorations of Korean

- steel plate girder bridges”, *Proc. Korean Soc. Stl. Const.*, **32-40**.
- Lam, H.F., Ko, J.M. and Wong, C.W. (1998), “Localization of damaged structural connections based on experimental modal and sensitivity analysis”, *J. Sound. Vib.*, **210**(1), 91-115.
- Levis, P and Gay, D. (2009), *TinyOS Programming*, Cambridge University Press, New York.
- Liang, C., Sun, F.P. and Rogers, C.A. (1996), “Electro-mechanical impedance modeling of active material systems”, *Smart Mater. Struct.*, **5**(2), 171-186.
- Lynch, J.P., Law, K.H., Kiremidjian, A.S., Carryer, E., Farrar, C.R., Sohn, H., Allen, D.W., Nadler, B. and Wait, J.R. (2004), “Design and performance validation of a wireless sensing unit for structural monitoring applications”, *Struct. Eng. Mech.*, **17**(34), 393-408.
- Lynch J.P., Wang, W., Loh, K.J., Yi, J.H. and Yun, C.B. (2006), “Performance monitoring of the geumdang bridge using a dense network of high-resolution wireless sensors”, *Smart Mater. Struct.*, **15**(6), 1561-1575.
- Mascarenas, D.L., Todd, M.D., Park, G. and Farrar, C.R., (2007), “Development of an impedancebased wireless sensor node for structural health monitoring”, *Smart Mater. Struct.*, **16**(6), 2137-2145.
- Mascarenas, D.L., Park, G., Farinholt, K.M., Todd, M.D. and Farrar, C.R. (2009), “A low-power wireless sensing device for remote inspection of bolted joints”, *J. Aerospace Eng.*, **233**(5), 565-575.
- Memsic Co. (2010), “Datasheet of ISM400”, Available from: <<http://www.memsic.com>>.
- Nagayama, T. (2007), “*Structural health monitoring using smart sensors*”, Ph.D Dissertation, University of Illinois at Urbana-Champaign, UC, USA.
- Nagayama, T., Sim, S.H., Miyamori, Y. and Spencer, B.F. (2007.) “Issues in structural health monitoring employing smart sensors”, *Smart Struct. Syst.*, **3**(3), 299-320.
- Nagayama, T., Spencer, B.F. and Rice, J.A. (2009), “Autonomous decentralized structural health monitoring using smart sensors”, *Struct. Control Health Monit.*, **16**(7-8), 842-859.
- Park, J.H., Kim, J.T., Hong, D.S., Mascarenas, D. and Lynch, J.P. (2010), “Autonomous smart sensor nodes for global and local damage detection of prestressed concrete bridges based on accelerations and impedance measurements”, *Smart Struct. Syst.*, **6**(56), 711-730.
- Park, S., Yun, C.B., Roh, Y. and Lee, J. (2005), “Health monitoring of steel structures using impedance of thickness modes at PZT patches”, *Smart Struct. Syst.*, **1**(4), 339-353.
- Park, G., Farrar, C.R., Scalea, F.L. and Coccia, S. (2006), “Performance assessment and validation of piezoelectric active-sensors in structural health monitoring”, *Smart Mater. Struct.*, **15**(6), 1673-1683.
- Rice, J.A. and Spencer, B.F. (2008), “Structural health monitoring sensor development for the imote2 platform”, *Proceedings of the SPIE*, 6932, San Diego.
- Rice, J.A., Mechitov, K., Sim, S.H., Nagayama, T., Jang, S., Kim, R., Spencer, B.F., Agha, G.A. and Fujino, Y. (2010), “Flexible smart sensor framework for autonomous structural health monitoring”, *Smart Struct. Syst.*, **6**(56), 423-438.
- Roh, Y., Kim, D.Y., Yang, S.H., Park, S. and Yun, C.B. (2005), “PZT-induced lamb waves and pattern recognitions for online health monitoring of joint steel plates”, *Key Eng. Mater.*, **321-323**, 146-151.
- Sazonov, E., Jha, R., Janoyan, K., Krishnamurthy, V., Fuchs, M. and Cross, K. (2006), “Wireless intelligent sensor and actuator network (WISAN): a scalable ultralowpower platform for structural health monitoring”, *Proceedings of the SPIE*, 6177, San Diego.
- SHMA User Guide (2010), Available from: <<http://shm.cs.uiuc.edu/documentation.html>>.
- Sim, S.H. and Spencer, B.F. (2007), “Multiscale sensing for structural health monitoring”, *Proceedings of the World Forum on Smart Material and Smart Structure Technology*, Chongqing & Nanjing, China.
- Sohn, H., Farrar, C.R., Hunter, N.F. and Worden, K. (2001), “Structural health monitoring using statistical pattern recognition techniques”, *J. Dyn. Syst. Meas. Control.*, **123**(4), 706-711.
- Sohn, H., Farrar, C.R., Hemez, F.M., Shunk, D.D., Stinemat, D.W. and Nadler, B.R. (2003), “*A review of structural health monitoring literature: 1996-2001*”, Los Alamos National Laboratory Report, LA-13976-MS, Los Alamos, NM.
- Spencer, B.F., RuizSandoval, M.E. and Kurata, N. (2004), “Smart sensing technology: opportunities and challenges”, *Struct. Control Health Monit.*, **11**(4), 349-368
- Straser, E.G. and Kiremidjian, A.S. (1998), “*A modular, wireless damage monitoring system for structure*”, Technical Report 128, John A. Blume Earthquake Engineering Center, Stanford University, Stanford, CA.
- Studer, M. and Peters, K. (2004), “Multiscale sensing for damage identification”, *Smart Mater. Struct.*, **13**(2),

- 283-294.
- Sun, F.P., Chaudhry, Z.A., Rogers, C.A., Majmundar, M., and Liang, C. (1995). "Automated real-time structure health monitoring via signature pattern recognition", *Proceeding of the SPIE Conference on Smart Structures and Materials*, San Diego, USA.
- Taylor, S.G., Farinholt, K.M., Flynn, E.B., Figueiredo, E., Mascarenas, D.L., Park, G., Todd, M.D., Farrar, C.R. (2009), "A mobileagent based wireless sensing network for structural monitoring applications", *Meas. Sci. Technol.*, **20**(4), 1-14.
- Weng, J.H., Loh, C.H., Lynch, J.P., Lu, K.C., Lin, P.Y. and Wang, Y. (2008), "Outputonly modal identification of a cablestayed bridge using wireless monitoring systems", *Eng. Struct.*, **30**(7), 1820-1830.
- Yi, J.H. and Yun, C.B. (2004), "Comparative study on modal identification methods using output-only information", *Struct. Eng. Mech.*, **17**(3-4), 445-446.
- Yun, C.B., Yi, J.H. and Bahng, E.Y. (2001), "Joint damage assessment of framed structures using neural networks technique", *Eng. Struct.*, **23**(5), 425-435.
- Zimmerman, A.T., Shiraishi, M., Swartz, R.A. and Lynch, J.P. (2008), "Automated modal parameter estimation by parallel processing within wireless monitoring systems", *J. Infrastruct. Syst.*, **14**(1), 102-113.

CC